Electromechanical coupling in piezoelectric nanobeams due to the flexoelectric effect

You may also be interested in:

Electromechanical coupling in piezoelectric nanobeams due to the flexoelectric effect

Z D Zhou[1,2]**, C P Yang**[1]**, Y X Su**[3,5]**, R Huang**[4,5] **and X L Lin**[1]

[1] Department of Materials Science and Engineering, College of Materials, Xiamen University, Xiamen, 361005, People's Republic of China
[2] Fujian Provincial Key Laboratory of Advanced Materials, Xiamen University, Xiamen, 361005, People's Republic of China
[3] Chengyi University College, Jimei University, Xiamen, 361021, People's Republic of China
[4] Department of Aerospace Engineering and Engineering Mechanics, University of Texas, Austin, TX 78712, United States of America

E-mail: suyaxuan@jmu.edu.cn and ruihuang@mail.utexas.edu

Abstract
The flexoelectric effect is a coupling of polarization and strain gradient, which exists in a wide variety of materials and may lead to strong size-dependent properties at the nanoscale. Based on an extension to the classical beam model, this paper investigates the electromechanical coupling response of piezoelectric nanobeams with different electrical boundary conditions including the effect of flexoelectricity. The electric Gibbs free energy and the variational principle are used to derive the governing equations with three types of electrical boundary conditions. Closed-form solutions are obtained for static bending of cantilever beams. The results show that the normalized effective stiffness increases with decreasing beam thickness in the open circuit electrical boundary conditions with or without surface electrodes. The induced electric potential due to the flexoelectric effect is obtained under the open circuit conditions, which may be important for sensing or energy harvesting applications. An intrinsic thickness depending on the material properties is identified for the maximum induced electric potential. The present results also show that flexoelectricity has a more significant effect on the electroelastic responses than piezoelectricity at the nanoscale. Our analysis in the present study can be useful for understanding of the electromechanical coupling in nanobeams with flexoelectricity.

Keywords: flexoelectric effect, piezoelectric nanobeam, electrical boundary, electromechanical coupling, induced electric potential

(Some figures may appear in colour only in the online journal)

1. Introduction

Electromechanical coupling of materials has been widely used in the nanoelectromechanical systems (NEMSs) such as resonators, sensors, actuators and energy harvesters [1]. The traditional electromechanical coupling mechanisms include piezoelectricity and electrostriction. Piezoelectricity, which generally assumes a linear relationship between electric field and strain, exists only in non-centrosymmetric dielectric materials. However, the strain gradient or nonuniform strain distributions could break the local inversion symmetry, which induces polarization even in centrosymmetric dielectric materials. This phenomenon is called flexoelectricity, which exists in liquid crystals, solid dielectrics and living membranes [2–4]. The flexoelectric effect is typically weak compared to the piezoelectric effect in bulk materials. However, the strain gradient is inversely proportional to the length scale of structures and could become very large in nanoscales. Since the induced polarization by the flexoelectric effect is proportional to the strain gradient, the flexoelectric effect could be significant at the nanoscale and should be considered in studying the electromechanical coupling in nano-devices.

---

[5] Authors to whom any correspondence should be addressed.

Mashkevich and Tolpygo [5] first predicted the flexoelectric effect and Tagantsev [6] studied the flexoelectric effect in bulk crystals theoretically. Ma and Cross [7–9] conducted a series of experiments to measure the flexoelectric coefficients of piezoelectric beams. They reported giant flexoelectric coefficients with high dielectric permittivity in ferroelectric materials. Kwon *et al* [10] determined experimentally the flexoelectric coefficients of barium strontium titanate (BST) thin films. They found that the transverse flexoelectric coefficient has a very large value at Curie temperature (∼28 °C). Garten and Trolier-McKinstry [11] found that the flexoelectricity could be enhanced through residual ferroelectricity in BST ceramics above the global phase transition temperature. Recently, several comprehensive reviews on flexoelectricity of solid crystals, thin films, polymers and living membranes have been published [12–14]. Jiang *et al* [15] summarized the flexoelectricity in various materials with applications in sensors and actuators as well as their capability of tuning the ferroelectric thin film properties.

With the development of nanotechnology, nanowires, nano-beams and nano-plates have been applied as the fundamental building blocks in NEMS. Due to the relatively large flexoelectric effect in dielectric materials at the nanoscale, the electromechanical coupling of the nano-beams and nano-plates with the flexoelectric effect has drawn a surge of interests. The influence of the flexoelectricity on the electromechanical coupling properties, such effective bending rigidity and effective piezoelectricity, of nano-beams and nano-plates has been studied. Based on the linear piezoelectricity theory developed by Toupin [16], Majdoub *et al* [17, 18] analyzed the model problem of a nanoscale cantilever beam and discussed the role of flexoelectricity in both piezoelectric and non-piezoelectric nanostructures. They reported that the 'effective' or 'apparent' piezoelectric coefficient and elastic modulus have significant size-dependence due to the flexoelectric effect. They also verified their predictions through atomistic calculations on BaTiO$_3$ nanobeams. Shen and Hu [19] have established a theoretical framework by a variational principle for nanosized dielectrics including the electrostatic force, flexoelectricity and surface effects. They also considered the electric field-strain gradient coupling in the electric Gibbs free energy density to incorporate the flexoelectric effect for nanoscale dielectrics [20]. Based on the internal energy density function, Yan and Jiang [21] investigated the influence of the flexoelectric effect on the electromechanical coupling properties of bending piezoelectric nanobeams. They reported that the flexoelectric effect was sensitive to the direction of applied electric potential on the surface electrodes. Considering the flexoelectric and surface effects, Zhang and Jiang [22] studied the size-dependent electromechanical coupling of piezoelectric ceramics at the nanoscale. In their work, the internal energy density function and a modified Kirchhoff plate model have been used to derive the governing equations and the corresponding boundary conditions. Based on the electric Gibbs energy, Liang *et al* [23] established a Bernoulli–Euler beam model for piezoelectric beams including the surface and flexoelectric effects. In their study, the open circuit electrical condition without surface electrodes, i.e. zero electric displacement on

the surfaces, was assumed. They found that the flexoelectric effect has a significant influence on the effective bending rigidity of piezoelectric nanowires. Mao and Purohit [24] derived the governing equations for a flexoelectric solid considering strain-gradient elasticity and proved a reciprocal theorem for flexoelectric materials. The flexoelectric effects of bending piezoelectric nanobeams and nanoplates have been investigated by analytical methods in open circuit and closed circuit electrical boundary conditions. The third electrical boundary condition, i.e. the surface electrodes with different electric potentials as a result of mechanical deformation due to the flexoelectric effect, is also interesting. To interpret the two-way flexoelectric coupling and complex geometries in the experiments, Abdollahi *et al* [25] analyzed computationally the flexoelectric effect in dielectric solids using smooth meshfree basis functions in a Galerkin method. They reported that the effective bending rigidity of the piezoelectric beam with flexoelectricity always increases with decreasing thickness. However, to our knowledge, this effect has not been considered by any analytical method.

The objective of the present study is to investigate the electromechanical coupling response of piezoelectric nanobeams with flexoelectric effects under three electrical boundary conditions: open circuit without surface electrodes (OC), closed circuit with a fixed external electric potential (CCF), and open circuit with surface electrodes and an induced electric potential by mechanical deformation (OCI). The constitutive equations of piezoelectric solids with the flexoelectric effect are derived. The electric Gibbs free energy and the variational principle are used to derive the governing equations of nanobeams with the three electrical boundary conditions. The normalized effective stiffness, the induced electric potential, electric field and polarization distributions in the beams are analyzed and discussed, emphasizing the influence of flexoelectricity on the electromechanical coupling response.

2. Constitutive equations of piezoelectric solids with the flexoelectric effect

For piezoelectric materials with the flexoelectric effect, the mathematical modeling based on the extended linear theory is employed. For simplicity, the contributions of the fifth and sixth order strain gradient elasticity are neglected [17, 23]. The electric Gibbs free energy density of a piezoelectric solid can be written as [20, 25]:

$$H = -\frac{1}{2}\kappa_{ij}E_iE_j + \frac{1}{2}c_{ijkl}\varepsilon_{ij}\varepsilon_{kl} - e_{ijk}E_i\varepsilon_{jk}$$
$$+ f_{ijkl}E_i\varepsilon_{jk,l} + d_{ijkl}E_{i,j}\varepsilon_{kl}, \quad (1)$$

where E_i is the electric field vector and ε_{ij} is the strain tensor; κ_{ij} is the second-rank dielectric tensor, c_{ijkl} is the fourth-rank elastic modulus, e_{ijk} is the third-rank piezoelectric tensor, d_{ijkl} and f_{ijkl} are the fourth-rank flexoelectric tensors. In particular, d_{ijkl} is the converse flexoelectric tensor, coupling the gradient of electric field ($E_{i,j}$) and the strain, while f_{ijkl} is the direct flexoelectric tensor, coupling the strain gradient ($\varepsilon_{jk,l}$) and the

electric filed. Using integration by parts, Sharma *et al* [26] defined an effective flexoelectric tensor, h_{ijkl}, which combines the two fundamentally different coupling phenomena (strain-polarization gradient coupling and strain gradient-polarization coupling) as part of the Helmholtz free energy density function in terms of strain and polarization. Here, in terms of the strain and electric field, the two coupling terms in equation (1) for the electric Gibbs free energy density function may also be combined into one term with an effective flexoelectric tensor [25]: $\mu_{ijkl} = d_{iljk} - f_{ijkl}$. As a result, the electric Gibbs free energy can be rewritten as

$$H = -\tfrac{1}{2}\kappa_{ij}E_iE_j + \tfrac{1}{2}c_{ijkl}\varepsilon_{ij}\varepsilon_{kl} - e_{ijk}E_i\varepsilon_{jk} - \mu_{ijkl}E_i\varepsilon_{jk,l}. \quad (2)$$

Under an infinitesimal deformation, the constitutive equations for the piezoelectric solid with the flexoelectric effect can be derived from the electric Gibbs free energy as

$$\sigma_{ij} = \frac{\partial H}{\partial \varepsilon_{ij}} \quad = c_{ijkl}\varepsilon_{kl} - e_{kij}E_k,$$

$$D_i = -\frac{\partial H}{\partial E_i} = \kappa_{ij}E_j + e_{ijk}\varepsilon_{jk} + \mu_{ijkl}\varepsilon_{jk,l}, \quad (3)$$

where σ_{ij} is the classical Cauchy stress tensor and D_i is the electric displacement vector. Since $D_i = \epsilon_0 E_i + P_i$ and $\kappa_{ij} = \epsilon_0 \delta_{ij} + \chi_{ij}$, we obtain the electric polarization: $P_i = \chi_{ij}E_j + e_{ijk}\varepsilon_{jk} + \mu_{ijkl}\varepsilon_{jk,l}$, where ϵ_0 is the electric permittivity of vacuum and χ_{ij} denote the electric susceptibility of the material. In addition, the higher-order stress tensor arising from flexoelectricity is

$$\sigma_{ijk} = \frac{\partial H}{\partial \varepsilon_{ij,k}} = -\mu_{lijk}E_l. \quad (4)$$

Substituting equations (3) and (4) into equation (2), the electric Gibbs free energy H can be rewritten as

$$H = \tfrac{1}{2}\sigma_{ij}\varepsilon_{ij} + \tfrac{1}{2}\sigma_{ijk}\varepsilon_{ij,k} - \tfrac{1}{2}D_iE_i. \quad (5)$$

The total electrical enthalpy of the solids can then be written as [24, 25]

$$\mathcal{H} = \iiint H\,\mathrm{d}V + \oiint \varpi\phi\,\mathrm{d}S - \oiint t_iu_i\,\mathrm{d}S - \oiint r_iv_i\,\mathrm{d}S, \quad (6)$$

where ϖ and ϕ are surface charge density and electric potential, t_i and u_i are the traction and displacement on the surface, r_i and v_i are the higher-order traction and normal derivative of displacement on the surface [24, 25]. In general, we have $r_i = \sigma_{ijk}n_jn_k$ and $v_i = u_{i,j}n_j$, where n_j is the outward unit normal vector on the surface.

3. A Bernoulli–Euler beam model with the flexoelectric effect

In this section, the classical Bernoulli–Euler beam model is adopted to study bending piezoelectric nanobeams with different electric boundary conditions. A cantilever piezoelectric nanobeam with the length L, the width b and the thickness h is depicted in figure 1, which is mechanically fixed at the left end and loaded by distributed lateral force, $q(x_1)$. The three electrical boundary conditions considered here are OC, CCF and OCI conditions, respectively. In the OC condition, the
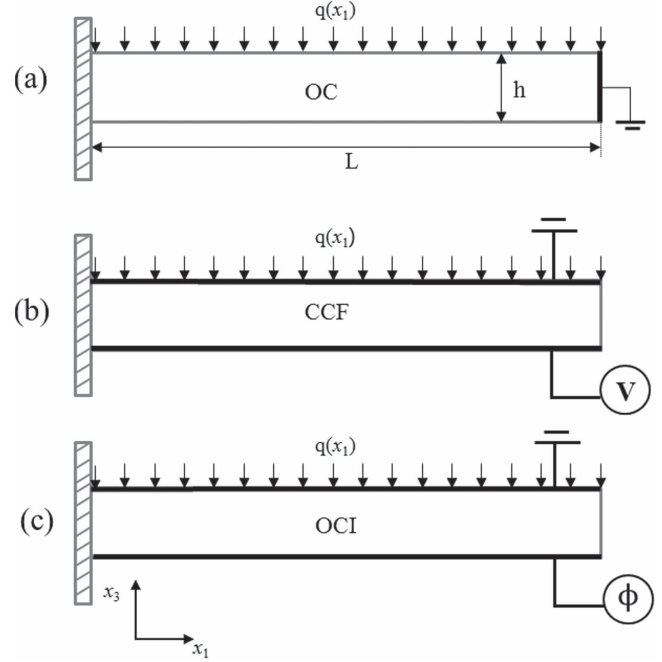

Figure 1. Schematics of cantilever piezoelectric nanobeams. (a) in the open circuit condition; (b) in the closed circuit condition with a fixed electric voltage V; (c) in the open circuit condition with surface electrodes and an induced electric potential ϕ.

electric potential is set to zero at the right-end [25] while the top and bottom surfaces are charge free ($\varpi = 0$). In the CCF condition, the top surface electrode is connected to the ground and the bottom surface electrode prescribes an external voltage V. This is a classical actuator model, which can deform against the mechanical load due to the electric load and convert electrical energy to do mechanical work. In the OCI condition, the top surface electrode is grounded and the bottom surface electrode undergoes a change of electric potential as a result of mechanical deformation. This is a classical sensor model and may also be used for energy harvesting by converting mechanical energy to electricity.

Following the Bernoulli–Euler beam model, the displacement of the beam can be expressed as [21, 23, 25, 27]

$$u = -x_3\frac{\partial w}{\partial x_1}, \ v = 0, \ w = w(x_1), \quad (7)$$

where v is the displacement in the x_2 direction and set to be zero as in plane strain elasticity. The non-zero components of the strain and strain gradients are obtained as

$$\varepsilon_{11} = -x_3\frac{\mathrm{d}^2w}{\mathrm{d}x_1^2}, \ \varepsilon_{11,3} = -\frac{\mathrm{d}^2w}{\mathrm{d}x_1^2}, \ \varepsilon_{11,1} = -x_3\frac{\mathrm{d}^3w}{\mathrm{d}x_1^3}. \quad (8)$$

Note that the strain gradient $\varepsilon_{11,3} = -\mathrm{d}^2w/\mathrm{d}x_1^2$ is essentially the curvature of the beam while $\varepsilon_{11,1} = -x_3\mathrm{d}^3w/\mathrm{d}x_1^3$ is proportional to the gradient of curvature. The latter is assumed to be small compared to the former in the Bernoulli-Euler beam model and may be neglected for a slender beam (i.e., $L \gg h$). For the same reason, the electric variables (electric field and electric displacement) in a slender beam are predominantly in the thickness direction, while the electric field (E_1) and electric displacement (D_1) components in the

length direction are negligible in three electrical boundary conditions [17, 21, 23, 28]. Thus, in the present paper, only the components E_3 and D_3 are considered for the electric variables.

By the constitutive relations in equations (3) and (4), the corresponding components of Cauchy stress, high-order stress and electric displacement can be obtained as

$$\begin{aligned}
\sigma_{11} &= c_{11}\varepsilon_{11} - e_{311}E_3, \\
\sigma_{113} &= -\mu_{3113}E_3, \\
D_3 &= \kappa_{33}E_3 + e_{311}\varepsilon_{11} + \mu_{3113}\varepsilon_{11,3}.
\end{aligned} \tag{9}$$

In the absence of free body charges, Gauss's law of electrostatics requires that

$$D_{3,3} = 0. \tag{10}$$

Substituting equation (9) into equation (10), we obtain

$$\frac{\partial^2 \Phi}{\partial x_3^2} = -\frac{e_{311}}{\kappa_{33}}\frac{\mathrm{d}^2 w}{\mathrm{d}x_1^2}, \tag{11}$$

where the electric potential Φ is related to the electric field by $E_3 = -\frac{\partial \Phi}{\partial x_3}$. Let $\Phi\left(x_3 = \frac{h}{2}\right) = V_1(x_1)$ and $\Phi\left(x_3 = -\frac{h}{2}\right) = V_2(x_1)$ on the top and bottom surfaces of the beam, respectively. Setting $\phi(x_1) = V_2(x_1) - V_1(x_1)$ and solving equation (11), we obtain

$$\Phi(x_1, x_3) = -\frac{e_{311}}{2\kappa_{33}}\frac{\mathrm{d}^2 w}{\mathrm{d}x_1^2}x_3^2 - \frac{\phi(x_1)}{h}x_3 + C(x_1), \tag{12}$$

where $C(x_1)$ is a function of x_1. Therefore, the electric field, electric displacement, stress, high-order stress and polarization can be obtained (see appendix for details), with which the electric Gibbs free energy density is obtained in terms of the deflection $w(x_1)$ and the surface electric potential $\phi(x_1)$. We note that $\phi(x_1)$ is assumed to be a slow-varying function of x_1 so that the electric field in the length direction of the beam is relatively small.

4. Static bending of a cantilever piezoelectric beam

By the variational principle [23], $\delta\mathcal{H} = 0$ is required for mechanical and electrostatic equilibrium of the nanobeam. With equation (A.6) along with equation (8), we obtain

$$\begin{aligned}
\iiint \delta H \mathrm{d}V &= \int_L^0 \left[\frac{bh^3}{12}\left(c_{11} + \frac{e_{311}^2}{\kappa_{33}}\right)\frac{\mathrm{d}^4 w}{\mathrm{d}x_1^4}\right. \\
&\quad \left. + \mu_{3113}b\frac{\mathrm{d}^2\phi(x_1)}{\mathrm{d}x_1^2}\right]\delta w \mathrm{d}x_1 \\
&\quad + \int_L^0 \left(\mu_{3113}b\frac{\mathrm{d}^2 w}{\mathrm{d}x_1^2} - \kappa_{33}b\frac{\phi(x_1)}{h}\right)\delta\phi \mathrm{d}x_1 \\
&\quad + \left[\frac{bh^3}{12}\left(c_{11} + \frac{e_{311}^2}{\kappa_{33}}\right)\frac{\mathrm{d}^2 w}{\mathrm{d}x_1^2} + \mu_{3113}b\phi(x_1)\right]\delta\left(\frac{\mathrm{d}w}{\mathrm{d}x_1}\right)\bigg|_0^L \\
&\quad - \left[\frac{bh^3}{12}\left(c_{11} + \frac{e_{311}^2}{\kappa_{33}}\right)\frac{\mathrm{d}^3 w}{\mathrm{d}x_1^3} + \mu_{3113}b\frac{\mathrm{d}\phi(x_1)}{\mathrm{d}x_1}\right]\delta w\bigg|_0^L.
\end{aligned} \tag{13}$$

Assume only the lateral force $q(x_1)$ loading on the top surface (figure 1) so that $\oiint t_i \delta u_i \mathrm{d}S = \int_0^L q(x_1)\delta w \mathrm{d}x_1$ and $\oiint r_i \delta v_i \mathrm{d}S = 0$. If there are no electrodes on the top, bottom surfaces and left end, the free charges ϖ are zero on these surfaces. Meanwhile, $\delta\phi = 0$ on the right end and $\varpi = 0$ on the left end. Thus we have $\oiint \varpi\delta\phi \mathrm{d}S = 0$ for the OC condition. If there are electrodes on the top and bottom surfaces and an external voltage V is applied, then $\delta\phi = 0$ on both surfaces. In this case, both ends are open circuit where the free charge ϖ is zero. So again we have $\oiint \varpi\delta\phi \mathrm{d}S = 0$ for the CCF condition. For the OCI condition, however, no external voltage V is applied to the electrodes. In this case, an electric potential ϕ is generated, which is independent of x_1 but would change with the mechanical load. Therefore, $\oiint \varpi\delta\phi \mathrm{d}S \neq 0$ for the OCI condition. In this section, we discuss these electrical boundary conditions and develop analytical solutions for bending of the piezoelectric nanobeams.

4.1. OC condition

Using equation (13) and the corresponding electric and mechanical boundary conditions, we obtain

$$\begin{aligned}
&\int_L^0 \left[\frac{bh^3}{12}\left(c_{11} + \frac{e_{311}^2}{\kappa_{33}}\right)\frac{\mathrm{d}^4 w}{\mathrm{d}x_1^4} + \mu_{3113}b\frac{\mathrm{d}^2\phi(x_1)}{\mathrm{d}x_1^2} - q(x_1)\right] \\
&\quad \times \delta w \mathrm{d}x_1 + \int_L^0 \left(\mu_{3113}b\frac{\mathrm{d}^2 w}{\mathrm{d}x_1^2} - \kappa_{33}b\frac{\phi(x_1)}{h}\right)\delta\phi \mathrm{d}x_1 \\
&\quad + \left[\frac{bh^3}{12}\left(c_{11} + \frac{e_{311}^2}{\kappa_{33}}\right)\frac{\mathrm{d}^2 w}{\mathrm{d}x_1^2} + \mu_{3113}b\phi(x_1)\right]\delta\left(\frac{\mathrm{d}w}{\mathrm{d}x_1}\right)\bigg|_0^L \\
&\quad - \left[\frac{bh^3}{12}\left(c_{11} + \frac{e_{311}^2}{\kappa_{33}}\right)\frac{\mathrm{d}^3 w}{\mathrm{d}x_1^3} + \mu_{3113}b\frac{\mathrm{d}\phi(x_1)}{\mathrm{d}x_1}\right]\delta w\bigg|_0^L = 0.
\end{aligned} \tag{14}$$

Due to the arbitrariness of δw and $\delta\phi$, the governing equations can be obtained as

$$G_E\frac{\mathrm{d}^4 w}{\mathrm{d}x_1^4} + \mu_{3113}b\frac{\mathrm{d}^2\phi(x_1)}{\mathrm{d}x_1^2} = q(x_1), \tag{15a}$$

$$\mu_{3113}\frac{\mathrm{d}^2 w}{\mathrm{d}x_1^2} - \kappa_{33}\frac{\phi(x_1)}{h} = 0, \tag{15b}$$

where $G_E = \frac{bh^3}{12}\left(c_{11} + \frac{e_{311}^2}{\kappa_{33}}\right)$ is the effective bending rigidity of the piezoelectric nanobeam without considering flexoelectricity. By equation (14), the boundary conditions at the ends of the cantilever beam are

$$w = \frac{\mathrm{d}w}{\mathrm{d}x_1} = 0 \quad (x_1 = 0), \tag{16a}$$

$$\begin{aligned}
&G_E\frac{\mathrm{d}^2 w}{\mathrm{d}x_1^2} + \mu_{3113}b\phi(x_1) = 0 \text{ and } G_E\frac{\mathrm{d}^3 w}{\mathrm{d}x_1^3} \\
&\quad + \mu_{3113}b\frac{\mathrm{d}\phi(x_1)}{\mathrm{d}x_1} = 0 \quad (x_1 = L).
\end{aligned} \tag{16b}$$

Combining equations (15a) and (15b), the governing equation for the cantilever piezoelectric nanobeam can be rewritten as

$$G_D \frac{\mathrm{d}^4 w}{\mathrm{d}x_1^4} = q(x_1), \tag{17}$$

where $G_D = G_E + \frac{\mu_{3113}^2}{\kappa_{33}} bh$ is the effective bending rigidity of the piezoelectric nanobeam with the flexoelectric effect, which is larger than G_E. Clearly, the normalized effective bending rigidity $G' = \frac{G_D}{G_E} = 1 + \frac{12\mu_{3113}^2}{\kappa_{33}c_{11}+e_{311}^2}\frac{1}{h^2}$ increases with decreasing thickness due to the flexoelectric effect. The same result was obtained in [23], where zero electric displacement condition on the beam surfaces was assumed. Since $\phi(x_1) = \frac{h\mu_{3113}}{\kappa_{33}}\frac{\mathrm{d}^2 w}{\mathrm{d}x_1^2}$ by equation (15b), the boundary conditions in equation (16b) can be simplified as

$$\frac{\mathrm{d}^2 w}{\mathrm{d}x_1^2} = \frac{\mathrm{d}^3 w}{\mathrm{d}x_1^3} = 0 \quad (x_1 = L). \tag{18}$$

4.2. CCF condition

In this case, $\phi(x_1)$ is a constant (ΔV) and independent of x_1 or the mechanical load. Using equation (13), we have

$$\int_L^0 \left[\frac{bh^3}{12}\left(c_{11} + \frac{e_{311}^2}{\kappa_{33}}\right)\frac{\mathrm{d}^4 w}{\mathrm{d}x_1^4} - q(x_1) \right]\delta w \mathrm{d}x_1$$
$$+ \left[\frac{bh^3}{12}\left(c_{11} + \frac{e_{311}^2}{\kappa_{33}}\right)\frac{\mathrm{d}^2 w}{\mathrm{d}x_1^2} + \mu_{3113}b\Delta V \right]\delta\left(\frac{\mathrm{d}w}{\mathrm{d}x_1}\right)\Big|_0^L$$
$$- \frac{bh^3}{12}\left(c_{11} + \frac{e_{311}^2}{\kappa_{33}}\right)\frac{\mathrm{d}^3 w}{\mathrm{d}x_1^3}\delta w\Big|_0^L = 0. \tag{19}$$

The governing equation can then be obtained as

$$G_E \frac{\mathrm{d}^4 w}{\mathrm{d}x_1^4} = q(x_1), \tag{20}$$

which is same as the result without the flexoelectric effect. While the boundary conditions at the left end ($x_1 = 0$) remain the same as equation (16a), the boundary conditions at the right end depend on the flexoelectric effect, i.e.

$$G_E \frac{\mathrm{d}^2 w}{\mathrm{d}x_1^2} + \mu_{3113}b\Delta V = 0 \text{ and } \frac{\mathrm{d}^3 w}{\mathrm{d}x_1^3} = 0 \quad (x_1 = L). \tag{21}$$

The effective bending rigidity G_E is independent of the flexoelectric effect, whereas the flexoelectric effect induces an effective bending moment through the boundary condition in equation (21). The present result is different from the previous result in [21], where the effective bending rigidity was derived from an internal energy density function. Their bending rigidity, which is affected by the flexoelectricity, is a smaller value than that of the conventional piezoelectric beam. When the beam thickness is several nanometers for barium titanate, their effective bending rigidity becomes negative [21]. It was argued that atomistic simulations should be used to determine the accurate properties at the nano scales. However, for some other materials with giant flexoelectric coefficients and low elastic moduli [10, 12], the effective bending rigidity as defined in [21] would become

negative when the beam thickness is less than several micrometers, which appears to be questionable. In contrast, the effective bending rigidity G_E in the present model remains positive under the CCF condition, independent of the beam thickness.

4.3. OCI condition

In this case, no external voltage is applied while the induced electric potential ϕ changes with the mechanical load on the surfaces. We assume $V_1 = 0$ and $V_2 = \phi$, which is independent on x_1 but depends on the mechanical load. For the cantilever beam subjected to the lateral load $q(x_1)$ on the top surface, we have

$$\int_L^0 \left[\frac{bh^3}{12}\left(c_{11} + \frac{e_{311}^2}{\kappa_{33}}\right)\frac{\mathrm{d}^4 w}{\mathrm{d}x_1^4} - q(x_1) \right]\delta w \mathrm{d}x_1$$
$$+ \int_L^0 \left(\mu_{3113}b\frac{\mathrm{d}^2 w}{\mathrm{d}x_1^2} - \kappa_{33}b\frac{\phi}{h} + b\varpi\right)\delta\phi \mathrm{d}x_1$$
$$+ \left[\frac{bh^3}{12}\left(c_{11} + \frac{e_{311}^2}{\kappa_{33}}\right)\frac{\mathrm{d}^2 w}{\mathrm{d}x_1^2} + \mu_{3113}b\phi \right]\delta\left(\frac{\mathrm{d}w}{\mathrm{d}x_1}\right)\Big|_0^L$$
$$- \left[\frac{bh^3}{12}\left(c_{11} + \frac{e_{311}^2}{\kappa_{33}}\right)\frac{\mathrm{d}^3 w}{\mathrm{d}x_1^3} \right]\delta w\Big|_0^L = 0. \tag{22}$$

Due to the arbitrariness of δw, the equilibrium equation is

$$G_E \frac{\mathrm{d}^4 w}{\mathrm{d}x_1^4} = q(x_1), \tag{23}$$

which is same as equation (20) for the CCF condition. The boundary conditions at the ends of the beam are also the same, except that the electric potential ϕ is to be determined under the OCI condition:

$$G_E \frac{\mathrm{d}^2 w}{\mathrm{d}x_1^2} + \mu_{3113}b\phi = 0 \text{ and } \frac{\mathrm{d}^3 w}{\mathrm{d}x_1^3} = 0 \quad (x_1 = L). \tag{24}$$

The difference between the OCI and CCF conditions lies in the electrical boundary condition on the electrode surfaces of the beam. For CCF, the applied voltage is specified and as a result there would be surface charges on the electrodes (e.g., supplied by a battery). For OCI, since $\delta\phi$ is independent of x_1 in equation (22), we obtain

$$\int_L^0 \left(\mu_{3113}\frac{\mathrm{d}^2 w}{\mathrm{d}x_1^2} - \kappa_{33}\frac{\phi}{h} + \varpi\right)\mathrm{d}x_1 = 0. \tag{25}$$

Under the open circuit condition, $\int_0^L \varpi \mathrm{d}x_1 = 0$ (no supply of charges to the electrodes) and thus

$$\int_L^0 \left(\mu_{3113}\frac{\mathrm{d}^2 w}{\mathrm{d}x_1^2} - \kappa_{33}\frac{\phi}{h}\right)\mathrm{d}x_1 = 0, \tag{26}$$

with which the induced electric potential ϕ can be determined. From equations (23) and (24), we obtain

$$\frac{\mathrm{d}^2 w}{\mathrm{d}x_1^2} = \frac{q}{2G_E}(x_1 - L)^2 - \frac{\mu_{3113}b\phi}{G_E}, \tag{27}$$

where the uniform lateral force q has been used for simplicity. Substituting equation (27) into the boundary condition (26), we obtain the induced electric potential due to the mechanical

bending as

$$\phi = \frac{\mu_{3113}hL^2}{6(\mu_{3113}^2 bh + G_E \kappa_{33})}q. \tag{28}$$

It is interesting to note that the contribution due to piezoelectricity appears to vanish for the induced electric potential in equation (28) except for its contribution to the effective bending rigidity G_E. This is a result of the pure bending deformation assumed in equation (7). In particular, the strain ε_{11} depends linearly on x_3 so that the electric field (E_3) induced by piezoelectricity takes opposite signs (but equal amplitude) in the upper and lower halves of the beam, leading to zero total electric potential ϕ by piezoelectricity. Substituting equation (28) into (24), the boundary condition of the cantilever beam is only related to material coefficients and the external mechanical load.

Solving the governing equations of the three conditions with corresponding boundary conditions, the deflections of the piezoelectric nanobeams are

$$w_{(1)} = \frac{q}{G_D}\left(\frac{x_1^4}{24} - \frac{x_1^3 L}{6} + \frac{x_1^2 L^2}{4}\right) \text{ for the OC condition,} \tag{29a}$$

$$w_{(2)} = \frac{q}{G_E}\left(\frac{x_1^4}{24} - \frac{x_1^3 L}{6} + \frac{x_1^2 L^2}{4}\right)$$
$$- \frac{\mu_{3113}b\Delta V x_1^2}{2G_E} \text{ for the CCF condition,} \tag{29b}$$

$$w_{(3)} = \frac{q}{G_E}\left(\frac{x_1^4}{24} - \frac{x_1^3 L}{6} + \frac{x_1^2 L^2}{4}\right) - \frac{q}{G_E}$$
$$\times \frac{x_1^2 L^2}{12 + h^2(c_{11}\kappa_{33} + e_{311}^2)/\mu_{3113}^2} \text{ for the OCI condition.} \tag{29c}$$

The analytical solutions obtained in the present study clearly show that the influences of flexoelectricity on the electroelastic behavior of the piezoelectric beams are different with different electrical boundary conditions. The deflections of the nanobeams due to the flexoelectric effect are always smaller than that without the flexoelectricity in the OC and OCI conditions. In contrast, the deflection of the nanobeams in the CCF condition can be smaller or larger, depending on the direction of the applied electric voltage.

5. Numerical results and discussion

In the present numerical examples, we assume the slenderness ratio of the beam is $L/h = 20$, and the width $b = h$. The electromechanical coupling response of the piezoelectric beam is loaded by a uniformly distributed pressure, $q = -0.1 \text{ N m}^{-1}$, on the top surface. The material BaTiO$_3$ is chosen to study the effects of flexoelectricity with different electric boundary conditions. The flexoelectric coefficient of BaTiO$_3$ can be obtained from experimental results [21, 29], which may also be estimated to be around 10^{-5}–10^{-7} C m^{-1} near the phase transition [8]. In this case, we choose $\mu_{3113} = 10^{-6} \text{ C m}^{-1}$. The other material properties for BaTiO$_3$ are: $c_{11} = 131 \text{GPa}$, $\kappa_{33} = 12.48 \text{ nC V}^{-1} \text{ m}^{-1}$, $e_{311} = -4.4 \text{ C m}^{-2}$ and $\chi_{33} = 12.46 \text{ nC V}^{-1} \text{ m}^{-1}$.

5.1. The normalized effective stiffness in three boundary conditions

As discussion in section 4, the effective bending rigidities of piezoelectric nanobeams with three electrical boundary conditions (OC, CCF and OCI) are different due to flexoelectricity. In the OC condition, the normalized effective bending rigidity $G' = \frac{G_D}{G_E}$ increases with decreasing thickness due to the flexoelectric effect. However, the apparent bending rigidity in the CCF and OCI conditions depends on the applied electric potential or the induced electric potential. In order to discuss the size-dependent effective elasticity due to flexoelectricity, we define the normalized effective stiffness [25]

$$Y = \frac{\frac{1}{2}\int \varepsilon_e c_{11} \varepsilon_e}{\frac{1}{2}\int \varepsilon_f c_{11} \varepsilon_f}, \tag{30}$$

where ε_f and ε_e are the strains obtained from the present model with and without consideration of flexoelectricity. In equation (30), the integral is over the volume of the beam. Figure 2(a) gives Y as a function of beam thickness h in three electric boundary conditions. It is observed that the normalized effective stiffness is greater than 1 and increases rapidly with decreasing beam thickness in the OC condition. In the OCI condition, the normalized effective stiffness increases slowly with decreasing beam thickness and approaches a plateau value as $h \rightarrow 0$. The reason is that the induced electric potential decreases with decreasing beam thickness when the beam thickness is small, which will be discussed further in the next section. In the CCF condition, the normalized effective stiffness first increases and then decreases with decreasing beam thickness when subjecting to a negative electric voltage. With consideration of flexoelectricity, the elastic strain energy is smallest as the thickness $h = 45 \text{ nm}$ with $V = -0.3$ V. Figure 2(b) shows the normalized deflection w/w_0 ($w_0 = qL^4/8G_E$ is the deflection at the free end without the flexoelectric effect) for the beam thickness $h = 30$, 45, and 100 nm, corresponding to the three points a, b and c in figure 2(a). From figure 2(b), we can see that the average curvature of the beam is the smallest for $h = 45 \text{ nm}$. When the thickness decreases, the normalized deflection has a large reversed deformation and the average curvature of the curve increases, in which the elastic energy would increase. When subjecting to a positive electric voltage, the normalized effective stiffness decreases monotonically with decreasing beam thickness. It is noted that the peak values of the normalized effective stiffness in OCI and CCF conditions are nearly the same, independent of the magnitude of the external negative electric voltage.

In order to discuss the effect of flexoelectricity on the effective bending stiffness of the beam, we defines the normalized bending stiffness K as

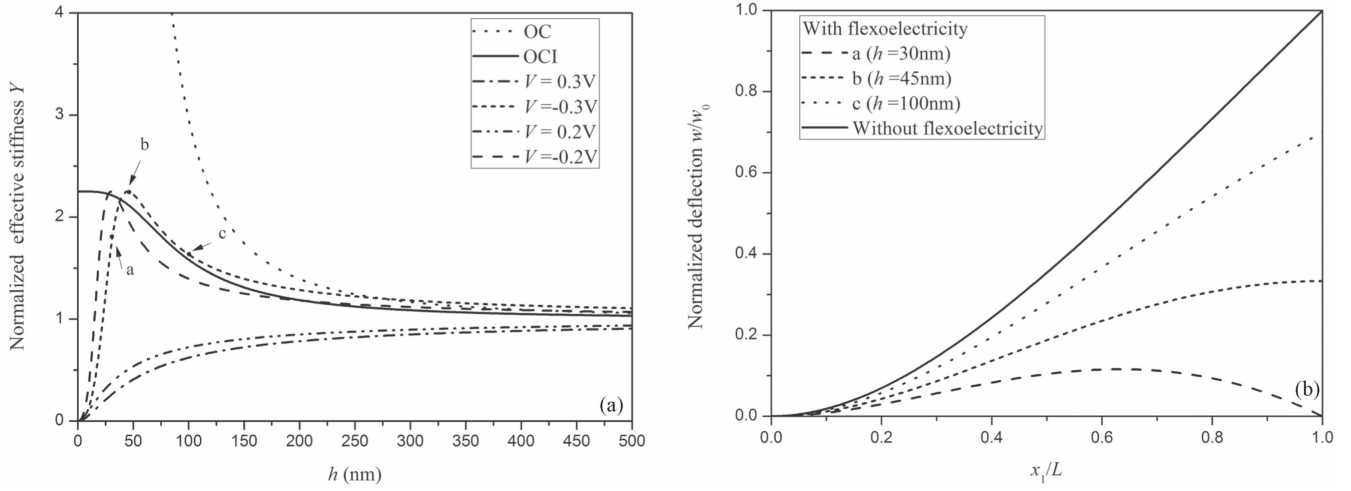$$K = \frac{\left|\int_0^L w_0 \, dx_1\right|}{\left|\int_0^L w_{(i)} \, dx_1\right|}. \tag{31}$$

Figure 2. (a) Variation of normalized effective stiffness Y as a function of the beam thickness h: OC, CCF and OCI conditions; (b) variation of the normalized deflection ($h = 30, 45, 100\,\mathrm{nm}$) in the CCF condition ($\Delta V = -0.3\,\mathrm{V}$).
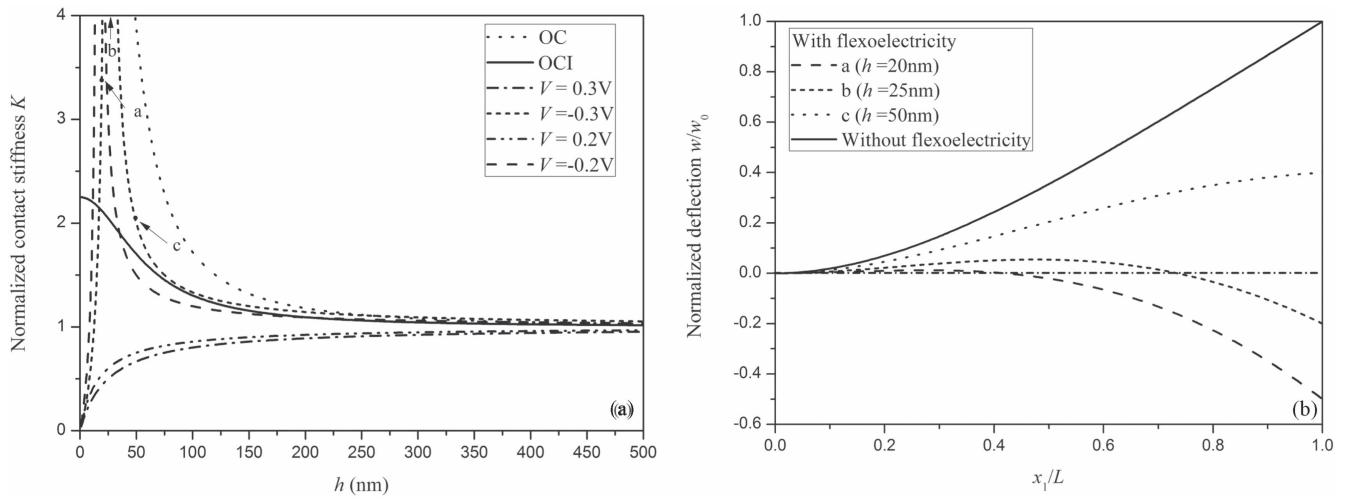

Figure 3. (a) Variation of the normalized stiffness K as a function of the beam thickness h: OC, CCF and OCI conditions; (b) variation of the normalized deflection ($h = 20, 25, 50\,\mathrm{nm}$) in CCF condition ($V = -0.3\,\mathrm{V}$).

In the three electric boundary conditions, the variation of the normalized stiffness K with the beam thickness h is showed in figure 3(a). It is observed that variation of the normalized stiffness K has the similar trend to the normalized effective stiffness Y in the OC and OCI conditions. However, in the CCF condition with $V = -0.3\,\mathrm{V}$, the average deflection along the beam length is nearly zero when the beam thickness is about 25 nm, which can be observed in figure 3(b). As a result, the normalized stiffness approaches infinity. When the beam thickness is sufficiently small, the large external voltage would cause the nanobeam to deflect reversely, in which case the absolute value of the average deflection along the beam length increases as shown in figure 3(b). It is clear from figures 2(a) and 3(a) that both Y and K approach 1 for all three electric boundary conditions with sufficiently large thickness, where the effect of flexoelectricity is negligible.

5.2. The induced electric potential, electric field and polarization in three boundary conditions

The induced electric potential can be very significant for nanobeams in the OCI condition. Moreover, the induced electric potential plays an important role in energy harvesting [30–32]. Equation (28) predicts that the induced electric potential depends nonlinearly on the beam thickness and the flexoelectric coefficient, as shown in figure 4. When $\alpha = L/h$ and $\beta = b/h$ are fixed, the induced electric potential approaches zero as the beam thickness approaches zero or infinity. In between, there exists a maximum induced electric potential at a particular thickness for each flexoelectric coefficient. By setting $\partial\phi/\partial h = 0$, we obtain the thickness h_o for the maximum induced electric potential:

$$h_o = \sqrt{\frac{12\mu_{3113}^2}{c_{11}\kappa_{33} + e_{311}^2}}. \tag{32}$$
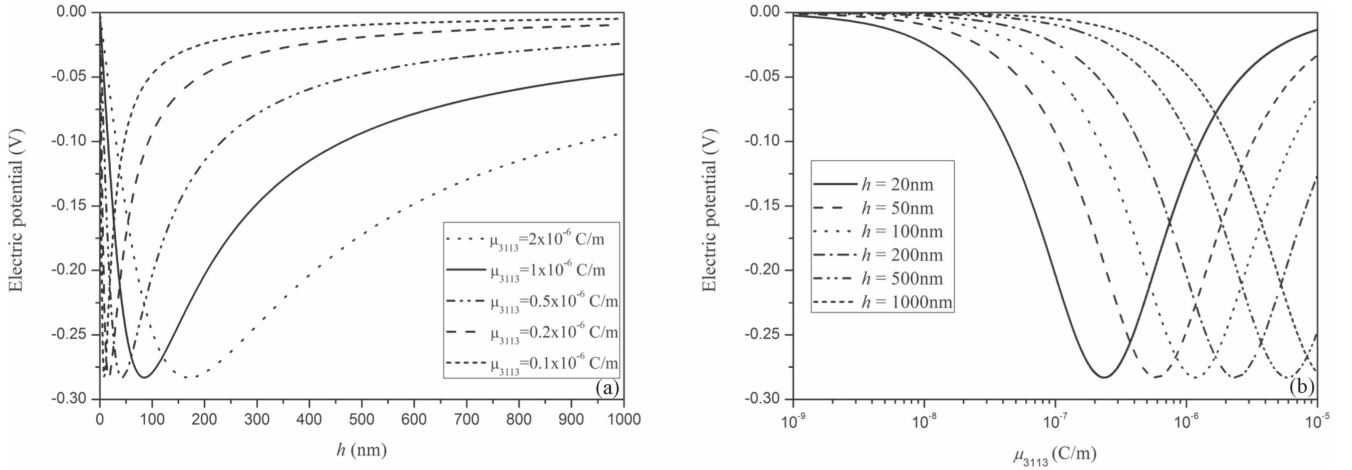
Figure 4. Variation of the induced electric potential with (a) beam thickness h for various flexoelectric coefficients and (b) flexoelectric coefficient μ_{3113} for different beam thicknesses.

Interestingly, the thickness h_o is independent of the aspect ratios (α and β) of the beam; it is an intrinsic length scale that depends on the material properties only. The optimal beam thickness increases with increasing flexoelectric coefficient with typical values around 100 nm (figure 4(a)). Similarly, for each beam thickness h, the magnitude of the induced electric potential is maximized at a particular flexoelectric coefficient (figure 4(b)). The optimal flexoelectric coefficient depends on the beam thickness as

$$\mu_o = h\sqrt{\frac{c_{11}\kappa_{33} + e_{311}^2}{12}}. \tag{33}$$

By equation (28), the induced electric potential approaches zero as the flexoelectric coefficient (μ_{3113}) approaches zero or infinity. This is a result of the competition between the two terms in the denominator of equation (28). When the first term dominates (i.e., $\mu_{3113}^2 bh \gg G_E\kappa_{33}$), the induced electric potential decreases with increasing flexoelectric coefficient. Under the OCI condition, the induced electric potential is to oppose the bending by the mechanical load. Hence, when the flexoelectric coefficient is large (or equivalently, thickness is small), the induced electric potential is small to oppose the same mechanical load. On the other hand, when the flexoelectric coefficient is very small (or thickness is very large), the second term dominates (i.e., $G_E\kappa_{33} \gg \mu_{3113}^2 bh$) and the induced electric potential increases linearly with the flexoelectric coefficient.

With equations (32) or (33), the maximum amplitude of the induced electric potential can be obtained as

$$\phi_{\max} = \frac{\alpha^2 q}{\beta\sqrt{12(c_{11}\kappa_{33} + e_{311}^2)}}. \tag{34}$$

With fixed values of α and β, the maximum induced electric potential predicted by equation (34) is independent of the flexoelectric coefficient or the beam thickness, which can be seen in figures 4(a) and (b) for $\alpha = 20$ and $\beta = 1$. Hence, for energy harvesting considering the flexoelectric effect, there exists an optimal beam thickness h_o for each material to reach the maximum output electric potential. After the thickness has been determined, the output electric potential increases with the ratio α^2/β.

In figure 5, the electric field E_3 of piezoelectric nanobeams (at $x_1 = L/2$) in the CCF condition is plotted for the beam thicknesses of 100 nm and 1000 nm, respectively. The results for these cases with and without flexoelectricity are compared. As the applied voltage is -0.3 V, the change of the electric field with flexoelectricity is smaller than that without the flexoelectricity. For the smaller thickness, the flexoelectric effect has a significant effect on the electric field as shown in figure 5(a). However, when the beam thickness increases to 1000 nm, the flexoelectric effect becomes negligible and the change of the electric field is mainly due to the piezoelectric effect and external voltage. In the OCI condition, the induced electric potential is uniform along the beam length. However, the electric field is a function of x_1 and x_3, which can be obtained from equation (A.1). Figure 6 presents the distribution of the electric field in the OCI condition, in which beam thickness is 100 nm. The magnitude of electric field is the greatest at the lower corner near the fixed end ($x_1 = 0$) as shown in figure 6(a). Figure 6(b) shows the electric field vector distribution in the whole beam. The results show that the magnitude of electric field decreases on the bottom surface and increases on the top surface from $x_1 = 0$ to $x_1 = L$. It should be noted that, since the nonlocal electrical coupling between the electric field and electric field gradient is neglected in the present study, the electric field varies linearly along the thickness direction without any nonlinear effect near the surfaces of the beam [22, 33].

For the CCF and OCI conditions, figures 7(a)–(c) shows the polarizations of the nanobeams varying with the beam thickness h. Figure 7(a) shows that the polarization is positive and decreases with increasing beam thickness at both the fixed end ($x_1 = 0$) and the free end ($x_1 = L$) with a positive external voltage $V = 0.3$ V. Without flexoelectricity, the polarization is induced primarily by the dielectric term (the third term on the right hand side of equation (A.5)) due to the electric potential, which is nearly independent of x_1 under the CCF condition. The first term of equation (A.5) is
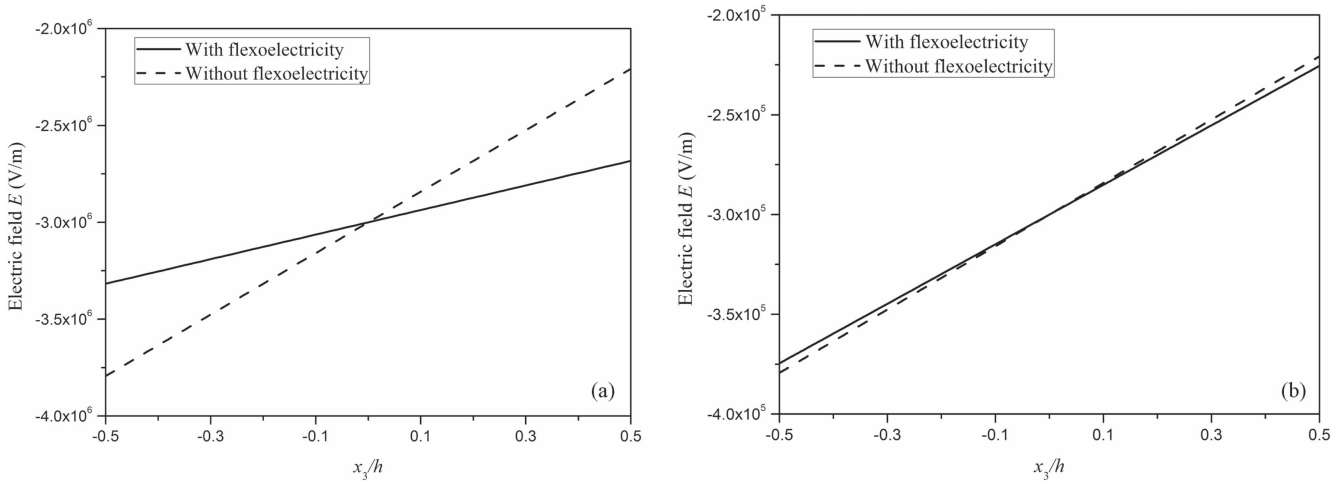
Figure 5. The electric field distribution along thickness direction in the CCF boundary condition ($V = -0.3$ V): (a) 100 nm, (b) 1000 nm.
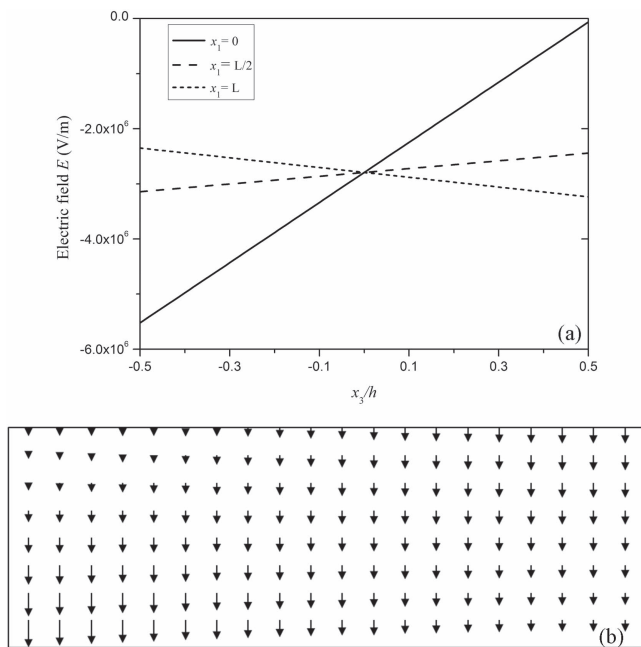

Figure 6. In the OCI condition, (a) the electric field distribution along the thickness direction at $x_1 = 0$, $L/2$, L and (b) the electric field vector distribution in the whole beam.

the polarization induced by piezoelectricity, which is very small, about 10^{-3}–10^{-4} C m^{-2} on top and bottom surfaces when the thickness is 20–500 nm. With flexoelectricity (the second term of equation (A.5)), the polarization is considerably larger. When the applied voltage is negative ($V = -0.3$ V), the polarization is positive at the fixed end ($x_1 = 0$) and negative at the free end ($x_1 = L$). The magnitude of polarizations at the fixed and free ends increase with decreasing beam thickness, as shown in figure 7(b). For the OCI condition, figure 7(c) shows the polarization as a function of the thickness at the fixed and free ends, respectively. In the present mechanical loading, the induced electric potential is always negative. As a result, the

polarization has the similar trend to the polarization in the CCF condition with a negative external voltage. Figure 7 also shows that the magnitude of polarization at the fixed end is larger than that at the free end. In contrast, if without flexoelectricity, the polarization induced by the piezoelectric effect is negligibly small (about 10^{-4} C m^{-2}) for the OCI condition.

6. Conclusions

In this paper, classical Bernoulli–Euler beam model is extended to investigate the flexoelectric effect in piezoelectric nanobeams with three different electric boundary conditions. The electric Gibbs free energy and a variational principle are used to derive the governing equations and boundary conditions. The static bending of cantilever beams are considered analytically. The analytical solutions of the deflections are obtained under different electrical boundary conditions. A nearly uniform electric potential distribution is generated by mechanical deformation due to the flexoelectric effect in the OCI condition. This uniform electric potential depends on the beam thickness and the flexoelectric coefficients with a peak value, which is very important to energy harvesting. Interestingly, there is an intrinsic length scale h_o, which depends on the material properties only. At this thickness h_o, the maximum output electric potential is dependent on the aspect ratios of the beam and independent on the flexoelectric coefficients. In addition, the normalized effective stiffness Y and normalized stiffness K due to the flexoelectric effect are discussed with respect to a range of beam thickness. The present results indicate that at the nanoscale, the induced electric potential, the electric field and polarization of nanobeams are considerably influenced by the flexoelectric effect. The present results could be helpful to understand the influence of the flexoelectric effect at nano-scales and to design nano-devices utilizing the flexoelectric effect.
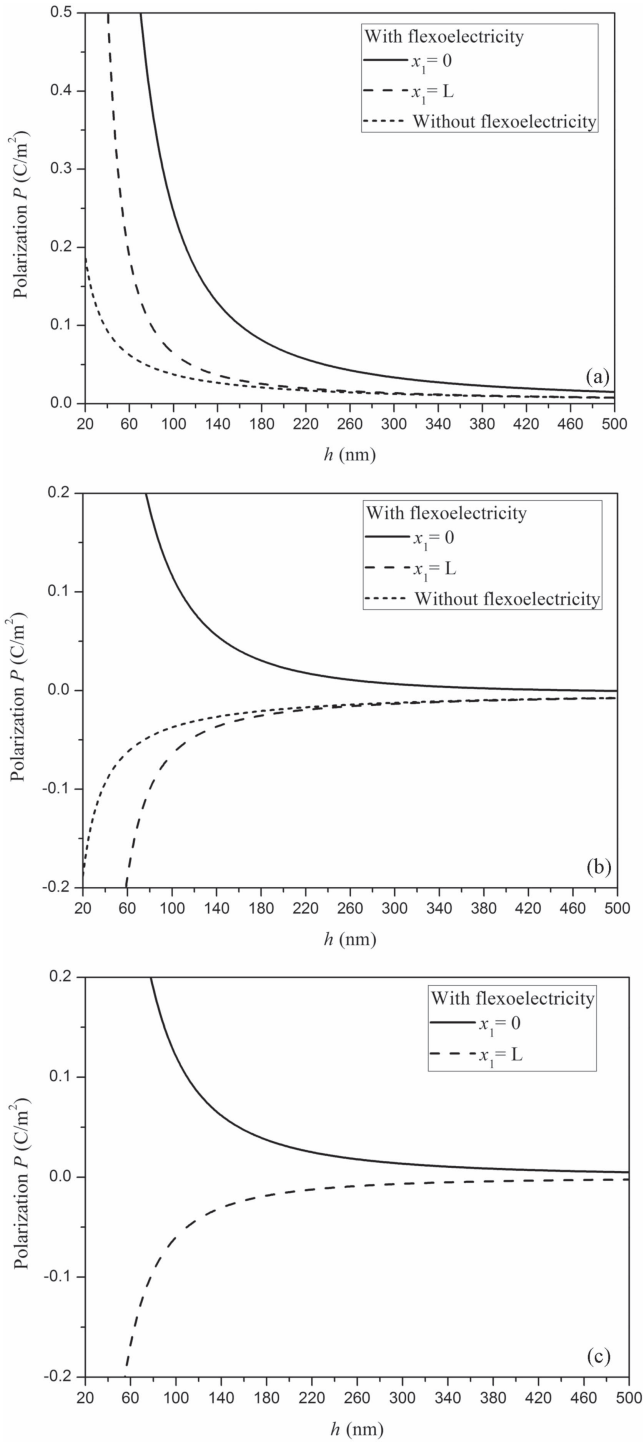
Figure 7. Variation of polarization with the beam thickness in (a) the CCF condition $V = 0.3$ V, (b) the CCF condition $V = -0.3$ V and (c) the OCI condition by induced electric potential.

Acknowledgments

Appendix A. The constitutive equations for a piezo-flexoelectric beam

Using equation (12), the electric field, electric displacement, stress, high-order stress and polarization of the beams can be obtained as:

$$E_3 = -\frac{e_{311}}{\kappa_{33}}\varepsilon_{11} + \frac{\phi(x_1)}{h}, \tag{A.1}$$

$$D_3 = \mu_{3113}\varepsilon_{11,3} + \kappa_{33}\frac{\phi(x_1)}{h}, \tag{A.2}$$

$$\sigma_{11} = \left(c_{11} + \frac{e_{311}^2}{\kappa_{33}}\right)\varepsilon_{11} - e_{311}\frac{\phi(x_1)}{h}, \tag{A.3}$$

$$\sigma_{113} = \frac{\mu_{3113}e_{311}}{\kappa_{33}}\varepsilon_{11} - \mu_{3113}\frac{\phi(x_1)}{h}, \tag{A.4}$$

$$P_3 = \frac{\epsilon_0 e_{311}}{\kappa_{33}}\varepsilon_{11} + \mu_{3113}\varepsilon_{11,3} + \chi_{33}\frac{\phi(x_1)}{h}. \tag{A.5}$$

Substituting the stress, strain, electric field, electric displacement, strain gradient and higher-order stress into equation (5), we obtain the electric Gibbs free energy as:

$$H = \frac{1}{2}\left(c_{11} + \frac{e_{311}^2}{\kappa_{33}}\right)\varepsilon_{11}^2 + \frac{e_{311}\mu_{3113}}{\kappa_{33}}\varepsilon_{11}\varepsilon_{11,3}$$
$$- \frac{\mu_{3113}\phi(x_1)}{h}\varepsilon_{11,3} - \frac{1}{2}\kappa_{33}\frac{\phi^2(x_1)}{h^2}. \tag{A.6}$$

References

[1] Yang J 2006 A review of a few topics in piezoelectricity *Appl. Mech. Rev.* **59** 335

[2] Gennes R G 1974 *The Physics of Liquid Crystals* (London: Oxford University Press)

[3] Indenbom V L, Loginov E B and Osipov M A 1981 Flexoelectric effect and crystal-structure *Kristallografiya* **26** 1157–62

[4] Petrov A G 2002 Flexoelectricity of model and living membranes *Biochim. Biophys. Acta-Biomembr.* **1561** 1–25

[5] Mashkevich V S and Tolpygo K B 1957 Electrical, optical and elastic properties of diamond type crystals: I *Sov. Phys. JETP* **32** 435–9

[6] Tagantsev A K 1991 Electric polarization in crystals and its response to thermal and elastic perturbations *Phase Transit.* **35** 119–203

[7] Ma W H and Cross L E 2001 Large flexoelectric polarization in ceramic lead magnesium niobate *Appl. Phys. Lett.* **79** 4420–2

[8] Ma W H and Cross L E 2005 Flexoelectric effect in ceramic lead zirconate titanate *Appl. Phys. Lett.* **86** 072905

[9] Ma W H and Cross L E 2006 Flexoelectricity of barium titanate *Appl. Phys. Lett.* **88** 232902

[10] Kwon S R, Huang W B, Shu L L, Yuan F G, Maria J P and Jiang X N 2014 Flexoelectricity in barium strontium titanate thin film *Appl. Phys. Lett.* **105** 142904

[11] Garten L M and Trolier-McKinstry S 2015 Enhanced flexoelectricity through residual ferroelectricity in barium strontium titanate *J. Appl. Phys.* **117** 094102

[12] Zubko P, Catalan G and Tagantsev A K 2013 Flexoelectric effect in solids *Ann. Rev. Mater. Res.* **43** 387–421

[13] Lee D and Noh T W 2012 Giant flexoelectric effect through interfacial strain relaxation *Phil. Trans. R. Soc* A **370** 4944–57

[14] Petrov A G 2006 Electricity and mechanics of biomembrane systems: flexoelectricity in living membranes *Anal. Chim. Acta* **568** 70–83

[15] Jiang X, Huang W and Zhang S 2013 Flexoelectric nano-generator: materials, structures and devices *Nano Energy* **2** 1079–92

[16] Toupin R A 1956 The elastic dielectric *Arch. Ration. Mech. Anal.* **5** 849–915

[17] Majdoub M S, Sharma P and Cagin T 2008 Enhanced size-dependent piezoelectricity and elasticity in nanostructures due to the flexoelectric effect *Phys. Rev.* B **77** 125424

[18] Majdoub M S, Sharma P and Cagin T 2009 Erratum: Enhanced size-dependent piezoelectricity and elasticity in nanostructures due to the flexoelectric effect *Phys. Rev.* B **79** 119904

[19] Shen S P and Hu S L 2010 A theory of flexoelectricity with surface effect for elastic dielectrics *J. Mech. Phys. Solids* **58** 655–77

[20] Hu S L and Sheng S P 2009 Electric field gradient theory with surface effect for nano-dielectrics *Comput. Mater. Continua* **13** 63–87

[21] Yan Z and Jiang L Y 2013 Flexoelectric effect on the electroelastic responses of bending piezoelectric nanobeams *J. Appl. Phys.* **113** 194102

[22] Zhang Z R and Jiang L Y 2014 Size effect on electromechanical coupling fields of a bending piezoelectric nanoplate due to surface effects and flexoelectricity *J. Appl. Phys.* **116** 134308

[23] Liang X, Hu S L and Shen S P 2014 Effects of surface and flexoelectric on a piezoelectric nanobeam *Smart Mater. Struct.* **23** 035020

[24] Mao S and Purohit P K 2014 Insights into flexoelectric solids from strain-gradient elasticity *J. Appl. Mech.—Trans. ASME* **81** 081004

[25] Abdollahi A, Peco C, Millan D, Arroyo M and Arias I 2014 Computational evaluation of the flexoelectric effect in dielectric solids *J. Appl. Phys.* **116** 093502

[26] Sharma N D, Landis C M and Sharma P 2010 Piezoelectric thin-film superlattices without using piezoelectric materials *J. Appl. Phys.* **108** 024304

[27] Yan Z and Jiang L Y 2011 Surface effects on the electromechanical coupling and bending behaviours of piezoelectric nanowires *J. Phys. D: Appl. Phys.* **44** 075404

[28] Wang G F and Feng X Q 2010 Effect of surface stresses on the vibration and buckling of piezoelectric nanowires *Europhys. Lett.* **91** 56007

[29] Giannakopoulos A E and Suresh S 1999 Theory of indentation of piezoelectric materials *Acta Mater.* **47** 2153–64

[30] Erturk A and Inman D J 2011 *Piezoelectric Energy Harvesting* (Chichester, West Sussex: Wiley)

[31] Erturk A and Inman D J 2009 An experimentally validated bimorph cantilever model for piezoelectric energy harvesting from base excitations *Smart Mater. Struct.* **18** 025009

[32] Deng Q, Kammoun M, Erturk A and Sharma P 2014 Nanoscale flexoelectric energy harvesting *Int. J. Solids Struct.* **51** 3218–25

[33] Liang X, Hu S L and Shen S P 2015 Size-dependent buckling and vibration behaviors of piezoelectric nanostructures due to flexoelectricity *Smart Mater. Struct.* **24** 105012